# UC Davis

## UC Davis Previously Published Works


### Title

The copper-sensing transcription factor Mac1, the histone deacetylase Hst1, and nicotinic acid regulate de novo NAD+ biosynthesis in budding yeast


### Permalink

https://escholarship.org/uc/item/6615j39s



### Journal

Journal of Biological Chemistry, 294(14)

### ISSN

0021-9258



### Authors

James Theoga Raj, Christol
Croft, Trevor
Venkatakrishnan, Padmaja
et al.



### Publication Date

2019-04-01

### DOI

10.1074/jbc.ra118.006987



### Copyright Information

This work is made available under the terms of a Creative Commons Attribution License, available at https://creativecommons.org/licenses/by/4.0/

Peer reviewed

eScholarship.org Powered by the California Digital Library
University of California

# The copper-sensing transcription factor Mac1, the histone deacetylase Hst1, and nicotinic acid regulate *de novo* $NAD^+$ biosynthesis in budding yeast

Received for publication, December 10, 2018, and in revised form, February 1, 2019 Published, Papers in Press, February 13, 2019, DOI 10.1074/jbc.RA118.006987

**Christol James Theoga Raj, Trevor Croft, Padmaja Venkatakrishnan, Benjamin Groth, Gagandeep Dhugga, Timothy Cater, and Su-Ju Lin**[1]

*From the Department of Microbiology and Molecular Genetics, College of Biological Sciences, University of California, Davis, California 95616*

Edited by John M. Denu

**NADH ($NAD^+$) is an essential metabolite involved in various cellular biochemical processes. The regulation of $NAD^+$ metabolism is incompletely understood. Here, using budding yeast (*Saccharomyces cerevisiae*), we established an $NAD^+$ intermediate–specific genetic system to identify factors that regulate the *de novo* branch of $NAD^+$ biosynthesis. We found that a mutant strain (*mac1*Δ) lacking Mac1, a copper-sensing transcription factor that activates copper transport genes during copper deprivation, exhibits increases in quinolinic acid (QA) production and $NAD^+$ levels. Similar phenotypes were also observed in the *hst1*Δ strain, deficient in the $NAD^+$-dependent histone deacetylase Hst1, which inhibits *de novo* $NAD^+$ synthesis by repressing *BNA* gene expression when $NAD^+$ is abundant. Interestingly, the *mac1*Δ and *hst1*Δ mutants shared a similar $NAD^+$ metabolism–related gene expression profile, and deleting either *MAC1* or *HST1* de-repressed the *BNA* genes. ChIP experiments with the *BNA2* promoter indicated that Mac1 works with Hst1-containing repressor complexes to silence *BNA* expression. The connection of Mac1 and *BNA* expression suggested that copper stress affects *de novo* $NAD^+$ synthesis, and we show that copper stress induces both *BNA* expression and QA production. Moreover, nicotinic acid inhibited *de novo* $NAD^+$ synthesis through Hst1-mediated *BNA* repression, hindered the reuptake of extracellular QA, and thereby reduced *de novo* $NAD^+$ synthesis. In summary, we have identified and characterized novel $NAD^+$ homeostasis factors. These findings will expand our understanding of the molecular basis and regulation of $NAD^+$ metabolism.**

$NAD^+$ and its reduced form NADH are primary redox carriers in cellular metabolism. $NAD^+$ is also a cosubstrate in protein modifications, such as protein deacetylation mediated by the sirtuins (Sir2 family proteins) and ADP-ribosylation mediated by the poly(ADP-ribose) polymerases. These protein modifications contribute to the maintenance and regulation of chromatin structure, DNA repair, circadian rhythm, metabolic responses, and life span (1–4). $NAD^+$ is also an $NADP^+$ precursor, which, like $NAD^+$, is carefully balanced with its reduced form NADPH to maintain a favorable redox state. Aberrant $NAD^+$ metabolism is associated with a number of diseases, including diabetes, cancer, and neuron degeneration (2, 3, 5–11). Administration of $NAD^+$ precursors, such as nicotinamide mononucleotide (NMN),[2] nicotinamide (NAM), nicotinic acid riboside, and nicotinamide riboside (NR), has been shown to ameliorate deficiencies related to aberrant $NAD^+$ metabolism in yeast, mouse, and human cells (3, 5–10, 12–15). However, the molecular mechanisms underlying the beneficial effects of $NAD^+$ precursor supplementation are not yet completely understood.

The $NAD^+$ pool is maintained by multiple $NAD^+$ biosynthesis pathways, which are conserved from bacteria to humans. Depending on the cell types, growth conditions, and availability of specific $NAD^+$ precursors, one pathway may dominate the others. In yeast, $NAD^+$ can be synthesized *de novo* from tryptophan or salvaged from intermediates, such as NA, NAM, and NR (Fig. 1*A*). In the *de novo* pathway, tryptophan is converted to QA through a series of enzymatic reactions catalyzed by Bna2, Bna7, Bna4, Bna5, and Bna1 (Fig. 1*A*) (16). QA is then phosphoribosylated by Bna6, producing nicotinic acid mononucleotide (NaMN). Because several steps in the *de novo* pathway require molecular oxygen as a substrate (Bna2, Bna4, and Bna1), cells grown under anaerobic conditions rely on the salvage pathways for $NAD^+$ synthesis (16). In the NA/NAM salvage pathway, yeast cells retrieve NAM from $NAD^+$ consumption reactions or uptake NA from the environment via NA transporter Tna1, leading to NaMN production. NaMN is also the converging point of the *de novo* pathway and NA/NAM salvage, which is converted to $NAD^+$ by NaMN adenylyltransferases (Nma1/2) (17) and glutamine-dependent $NAD^+$ syn-

This study was supported by NIGMS, National Institutes of Health, Grant GM102297. The authors declare that they have no conflicts of interest with the contents of this article. The content is solely the responsibility of the authors and does not necessarily represent the official views of the National Institutes of Health.

This article contains Table S1, Fig. S1, and Files S2 and S2.

[1] To whom correspondence should be addressed: Dept. of Microbiology and Molecular Genetics, University of California, One Shields Ave., Davis, CA 95616. Tel.: 530-754-6081; Fax: 530-752-9014; E-mail: slin@ucdavis.edu.

[2] The abbreviations used are: NMN, nicotinamide mononucleotide; NAM, nicotinamide; NA, nicotinic acid; NR, nicotinamide riboside; 3-HK, 3-hydroxykynurenine; 3-HA, 3-hydroxyanthranilic acid; QA, quinolinic acid; NaMN, nicotinic acid mononucleotide; KP, kynurenine pathway; KA, kynurenic acid; QA, quinolinic acid; 3-HK, 3-hydroxykynurenine; KYN, kynurenine; SD, synthetic minimal; SC, synthetic complete; 3-HA, 3-hydroxyanthranilic acid; GO, gene ontology; QPRT, quinolinate phosphoribosyl transferase; YPD, yeast extract-peptone-dextrose; Ab, antibody.



© 2019 James Theoga Raj et al. Published under exclusive license by The American Society for Biochemistry and Molecular Biology, Inc.

thetase (Qns1) (18) (Fig. 1*A*). NR salvage also contributes to NAD$^+$ synthesis. In yeast, NR is assimilated into NMN or NAM, catalyzed by the NR kinase Nrk1 (19) and nucleosidases Urh1/Pnp1/Meu1 (15), respectively. NMN is directly converted to NAD$^+$ via NMN adenylyltransferases (Nma1/2) (17), whereas NAM merges into the NA/NAM salvage pathway. It has also been shown that small NAD$^+$ precursors, such as NR, NA, NAM, and QA, constantly exit and re-enter yeast cells (20–22), which constitutes an extended NAD$^+$ precursor pool.

The complex and dynamic flexibility of NAD$^+$ precursors makes studying NAD$^+$ metabolism complicated. For example, NAM can both replenish NAD$^+$ pools and inhibit the activity of NAD$^+$-consuming enzymes. In addition, metabolites of the *de novo* pathway appear to have additional function. The *de novo* pathway is also known as the kynurenine pathway (KP) or tryptophan degradation pathway, and alterations of the KP metabolites have been linked to several brain disorders (11, 23). Interestingly, KP metabolites have been shown to exhibit both neuroprotective (kynurenic acid (KA)) and neurotoxic (QA and 3-hydroxykynurenine (3-HK)) effects (11, 23, 24) (Fig. 1*A*). KA is produced from kynurenine (KYN) by the KYN aminotransferase. Yeast cells also produce KA from KYN by the Aro8/9 aminotransferases (25); however, the function of KA in yeast remains unclear.

Studying the regulation of specific NAD$^+$ biosynthetic pathways has been challenging in part due to the redundancy and interconnections among them. Employing the properties of yeast cells that constantly release and retrieve small NAD$^+$ precursors (20–22), we have previously carried out precursor-specific genetic screens to identify novel NAD$^+$ homeostasis factors in yeast (1, 21, 26). In this study, we developed a QA release–based reporter system targeting the *de novo* branch of NAD$^+$ metabolism. The hypothesis was that cells with abnormal *de novo* NAD$^+$ synthesis activities would show altered QA release. The *mac1*Δ mutant was among the top hits that showed increased QA release. *MAC1* encodes a copper-sensing transcription factor (27–29), and our studies are the first to link Mac1 to NAD$^+$ homeostasis. Here, we characterized the *mac1*Δ mutants as well as additional factors that regulate the *de novo* pathway. Our studies help provide a molecular basis underlying the interconnection and cross-regulation of NAD$^+$ biosynthesis pathways.

## Results

### *A cell-based reporter assay to identify factors that modulate the de novo pathway*

*Saccharomyces cerevisiae* cells have been reported to secrete QA (22). We exploited this phenomenon and established a cross-feeding assay using the *bna4*Δ*npt1*Δ*nrk1*Δ mutant as "recipient cells" (which depend on QA for growth) and mutants of interest as "feeder cells." In this system, recipient cells cannot grow on standard growth media (which lack QA). When feeder cells are placed in proximity, feeder cell–released QA supports recipient cell growth by "cross-feeding." This assay determines relative levels of total QA released by feeder cells and can be considered as readout for the *de novo* pathway activity. As shown in Fig. 1*B*, recipient cells were spread onto synthetic minimal (SD) medium plates as a lawn. Next, WT, *bna1*Δ, *bna4*Δ, and *bna6*Δ feeder cells were spotted on top of the lawn and allowed to grow. Recipient cells near the feeder spots appeared as satellite colonies after 3 days, and the number and size of the satellite colonies positively correlate with the amount of QA released from the feeders. According to the function of Bna proteins in the *de novo* pathway (Fig. 1*A*), we expected *bna1*Δ and *bna4*Δ cells to release no QA and *bna6*Δ cells to release more QA. Indeed, as shown in Fig. 1*B*, both *bna1*Δ and *bna4*Δ feeder cells failed to support the growth of the recipient cells. In contrast, *bna6*Δ cells supported the growth of recipient cells more robustly than WT cells. We also tested a few mutants that have been associated with regulation of the *de novo* pathway. The NAD$^+$-dependent histone deacetylase Hst1 represses *BNA* gene expression. During NAD$^+$ deprivation, decreased Hst1 activity results in de-repression of *BNA* genes (30). Cells lacking *NPT1* and *TNA1* are defective in NA/NAM salvage and NA transport, respectively, and thus have decreased NAD$^+$ levels (31, 32). In addition, Tna1 was reported to also function as a QA transporter (22). Fig. 1*C* showed that *hst1*Δ, *npt1*Δ, and *tna1*Δ mutants all released more QA. These results demonstrated that mutants with altered QA levels and *de novo* activities could be identified using this system.

### *Transcription factor Mac1 is a novel NAD$^+$ homeostasis factor*

Next, we used the haploid yeast deletion collection as feeder cells to identify mutants with altered QA release (Fig. 1*D*). After incubation at 30 °C for 3 days, we scored the cross-feeding activity (which indicates the level of QA release) of each mutant by comparing the diameter of the cross-feeding zones with that of the WT. A relative QA release score was assigned to each mutant with the WT baseline score set at 0. Scores of −4, −3, and −2 indicate decreased QA release; scores of +2, +3, and +4 indicate increased QA release. To eliminate false-positives, mutants with scores of −4, −3, 3, and 4 (169 mutants) were re-examined. A total of 81 mutants passed the secondary screens on both SD and synthetic complete (SC) growth media (Table S1). Among the 12 mutants that show strongest QA release (score +4), most are known NAD$^+$ homeostasis factors, including *hst1*Δ, *npt1*Δ, *pnc1*Δ, *nat3*Δ, and their interacting partners (Table S1). *MAC1* encodes a copper-sensing transcription factor (27–29), which has not been associated with NAD$^+$ homeostasis. To verify that observed phenotypes are due to the featured mutations and not to secondary cryptic mutations in the deletion collection, we reconstructed all deletion mutants used in this study. Fig. 1*E* showed that *mac1*Δ released more QA, and deleting *HST1* did not further increase QA release in the *mac1*Δ mutant. Increased QA release correlates with increased levels of extracellular QA determined by quantitative liquid assays (Fig. 2*A*). Similar results were obtained using either *bna4*Δ*npt1*Δ*nrk1*Δ (Fig. 2*A*, *left*) or *bna1*Δ*npt1*Δ*nrk1*Δ (Fig. 2*A*, *right*) mutants as recipient cells. This suggests that QA is a major *de novo* pathway intermediate produced in feeder cells because *bna1*Δ*npt1*Δ*nrk1*Δ cells can only utilize QA, whereas *bna4*Δ*npt1*Δ*nrk1*Δ can utilize QA and additional intermediates, such as 3-hydroxykynurenine (3-HK)

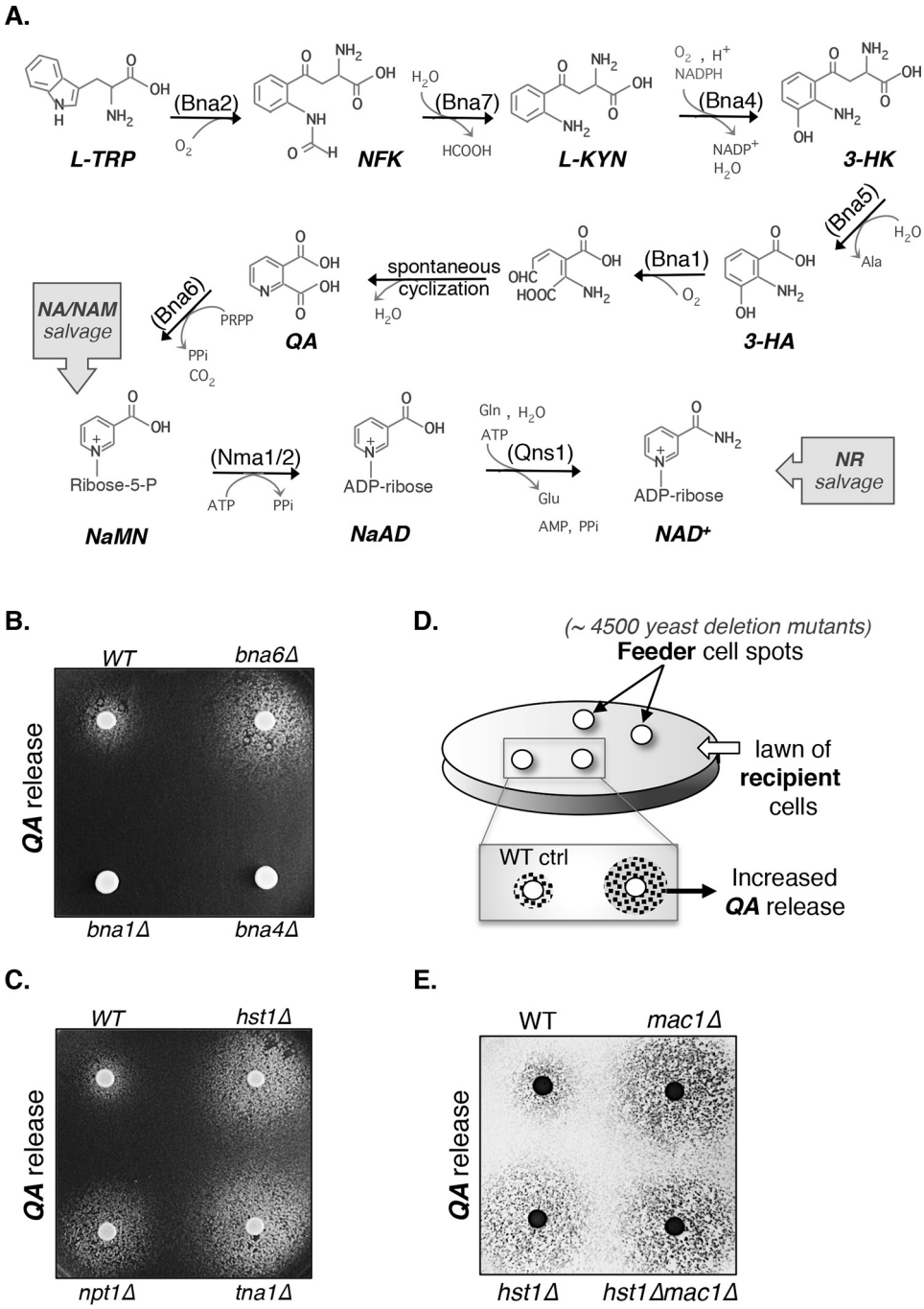


**Figure 1. Identification of yeast mutants with increased *de novo* NAD$^+$ synthesis activity.** *A*, simplified model of *Saccharomyces cerevisiae* NAD$^+$ synthesis pathways. The *de novo* NAD$^+$ synthesis is mediated by Bna2, -7, -4, -5, -1, and -6, leading to the production of NaMN. Yeast cells also produce NaMN from the *NA/NAM* salvage pathway, which is then converted to NAD$^+$ by Nma1/2 and Qns1. NR salvage contributes to NAD$^+$ synthesis in part depending on the NA/NAM salvage pathway. *L-TRP*, L-tryptophan; *NFK*, *N*-formylkynurenine; *NaAD*, deamido-NAD$^+$. Abbreviations of protein names are shown in *parentheses*. *Bna2*, tryptophan 2,3-dioxygenase; *Bna7*, kynurenine formamidase; *Bna4*, kynurenine 3-monooxygenase; *Bna5*, kynureninase; *Bna1*, 3-hydroxyanthranilate 3,4-dioxygenase; *Bna6*, quinolinic acid phosphoribosyl transferase; *Nma1/2*, NaMN/NMN adenylyltransferase; *Qns1*, glutamine-dependent NAD$^+$ synthetase. *B*, deletions of *BNA1 and BNA4* abolish QA release, whereas deletion of *BNA6* increases QA release. QA-dependent recipient cells (*npt1Δnrk1Δbna4Δ*) were plated onto SD plates as a lawn. Next, WT, *bna1Δ*, *bna4Δ*, and *bna6Δ* feeder cells were spotted on top of the lawn and allowed to grow for 3–4 days at 30 °C. The number and size of the satellite colonies surrounding the feeder spots positively correlate with the amount of QA released from the feeders. *C*, deletions of *HST1*, *NPT1*, and *TNA1* increase QA release. *D*, overview of the genetic screen to identify mutants with increased QA release. Haploid single-deletion mutants (feeder cells) were spotted onto a lawn of QA-dependent recipient cells, whose growth relies on QA released from the feeder cells in a dose-dependent manner. *E*, deletions of *MAC1 and HST1* confer increased QA release. For clarity, *inverse images* are shown.

and 3-hydroxyanthranilic acid (3-HA) (Fig. 1*A*). Interestingly, cells did not appear to retain excess QA intracellularly (Fig. 2*A*). Thus, increased QA may be converted to NAD$^+$ or released extracellularly. To examine whether Mac1 and Hst1 function in the same pathway to regulate NAD$^+$ homeostasis, we determined the levels of NR, NA/NAM, and NAD$^+$/NADH in WT, *mac1Δ*, *hst1Δ*, and *hst1Δmac1Δ* cells. Similar to the *hst1Δ* mutants, *mac1Δ* cells showed moderate increases in intracellu-

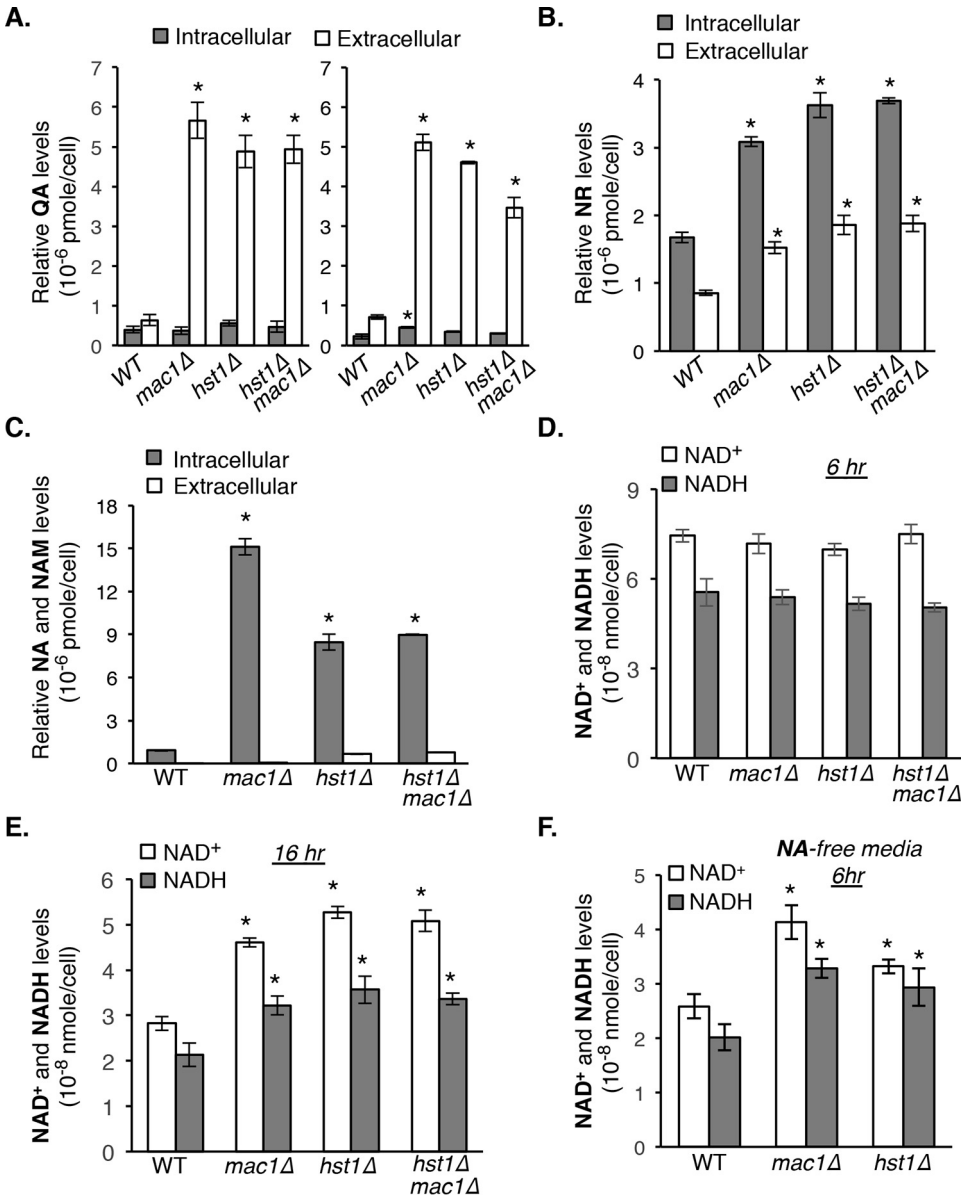


**Figure 2. Determination of QA and NAD$^+$ levels in cells lacking *HST1* and *MAC1*.** *A*, the *hst1*Δ and *mac1*Δ mutants show significant increases in QA levels. QA levels were determined in both growth media (released) and cell extracts (intracellular). Feeding of collected lysate and growth media to QA-dependent recipient cells was conducted in triplicate. Relative QA levels were determined using both *bna4*Δ*npt1*Δ*nrk1*Δ (*left*) and *bna1*Δ*npt1*Δ*nrk1*Δ (*right*) as QA-dependent recipient cells. *B*, the *hst1*Δ and *mac1*Δ mutants show increased NR levels. *C*, the *hst1*Δ and *mac1*Δ mutants show increased intracellular NA and NAM levels. *D*, measurements of intracellular NAD$^+$ levels. Deleting *HST1 and MAC1* does not increase NAD$^+$ levels in log-phase cells (6 h). *E*, deleting *HST1 and MAC1* significantly increases NAD$^+$ levels in late log-phase cells (16 h). *F*, deleting *HST1 and MAC1* significantly increases NAD$^+$ levels in log-phase cells (6 h) grown in NA-free media. *Error bars*, S.D. The *p* values are calculated using Student's *t* test (*, $p < 0.05$).

lar levels of NR (Fig. 2*B*) and NA/NAM (Fig. 2*C*). Increased expression of NA and NR transporters was reported in *hst1*Δ mutants (30, 33), which could contribute to observed increases of intracellular NR and NA/NAM. The *hst1*Δ mutant has also been shown to maintain higher steady-state NAD$^+$ levels (30). Consistent with this study, *mac1*Δ, *hst1*Δ, and *hst1*Δ*mac1*Δ mutants showed WT levels of NAD$^+$/NADH during early log-phase growth (6 h) (Fig. 2*D*); however, as cells entered late log phase (16 h), these mutants showed higher NAD$^+$/NADH levels when compared with WT cells (Fig. 2*E*). This result suggested that *mac1*Δ- and *hst1*Δ-induced QA production was indeed coupled to increased *de novo* NAD$^+$ synthesis. However, these mutants might also uptake more NA from the medium due to increased *TNA1* expression (Fig. 3*B*), which could contribute to observed increases in NAD$^+$/NADH levels. We therefore determined NAD$^+$/NADH levels in cells grown in NA-free medium to eliminate the contribution of NA. As shown in Fig. 2*F*, an increase in NAD$^+$/NADH level was still observed in *mac1*Δ and *hst1*Δ cells. Interestingly, we were able to observe this NAD$^+$/NADH increase in early log-phase cells grown in NA-free medium. These results were in line with the observations that the presence of NA (and/or NA salvage to NAD$^+$) inhibits *de novo* activity (30, 34). Overall, these studies showed a connection between increased QA production and increased *de novo* NAD$^+$ synthesis activity in *mac1*Δ and *hst1*Δ cells.

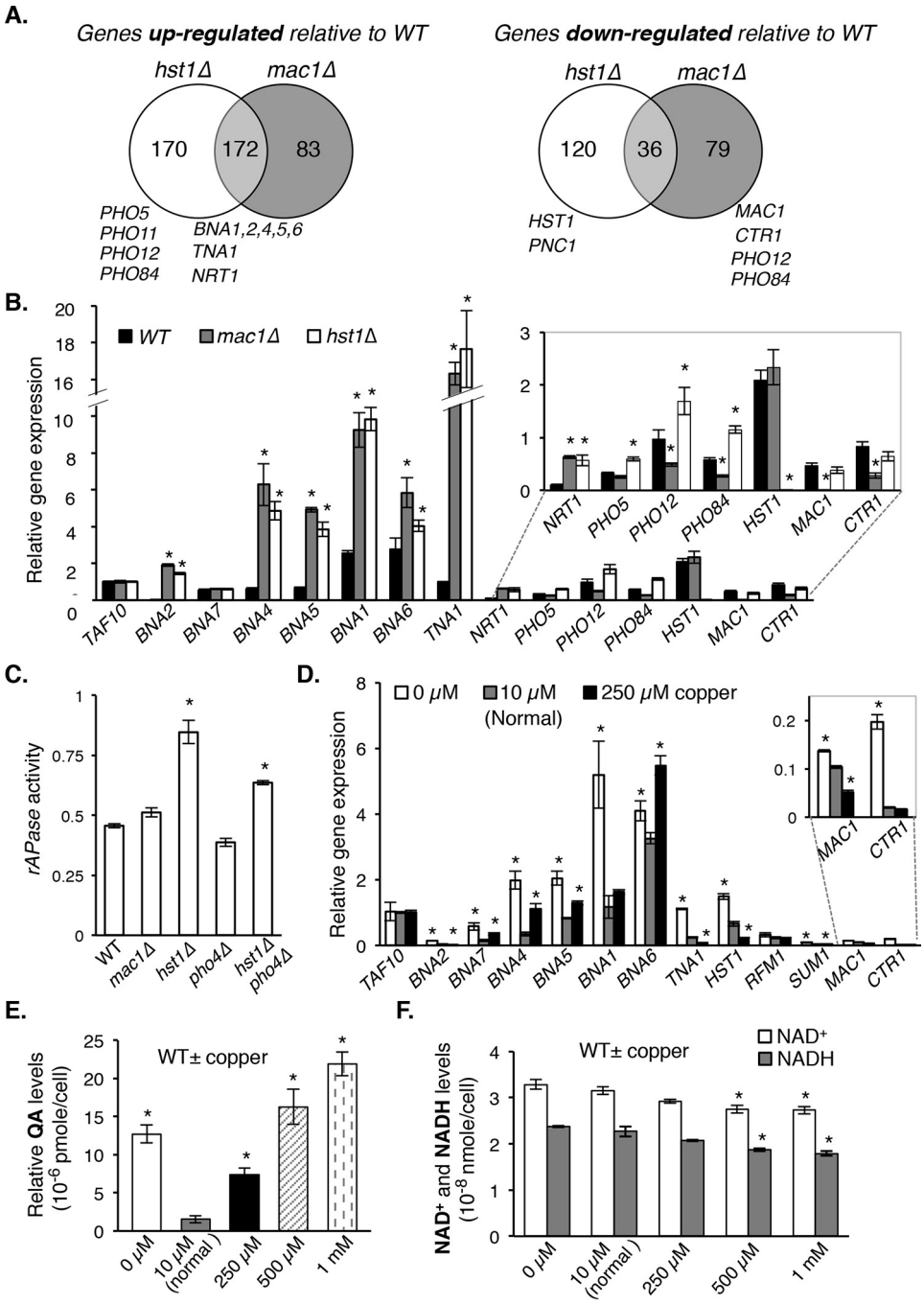


**Figure 3. Hst1 and Mac1 regulate gene expression of the *de novo* NAD$^+$ biosynthesis pathway.** *A*, gene expression profile analyses of WT, *hst1*Δ and *mac1*Δ cells. The Venn diagrams show genes that are up-regulated (*left*) or down-regulated (*right*) in the *hst1*Δ and *mac1*Δ mutants relative to WT. *de novo* NAD$^+$ biosynthesis–associated *BNA* genes are among the 172 genes co-up-regulated in *hst1*Δ and *mac1*Δ cells. *B*, validating *BNA* gene expression in WT, *hst1*Δ, and *mac1*Δ cells by qPCR. Results showed relative expression levels of *BNA*, *MAC1*, *HST1*, *SUM1*, *RFM1* (*SUM1* and *RFM1* encode components of the Hst1 protein complex), *TNA1*, and *CTR1* genes. Relative gene expression (normalized to *TAF10*) is shown. *C*, relative repressible acid phosphatase (*rAPase*, *Pho5*) activities in WT, *hst1*Δ, and *mac1*Δ cells. Increased *rAPase* activity in *hst1*Δ cells indicates increased *PHO* signaling activity. *D*, relative *BNA* gene expression in log-phase cells grown in copper-free (0 μM), nutritional copper level (10 μM, normal), and high-copper (250 μM) SD media. *E*, QA production is altered by high copper stress and copper deprivation. Results show relative levels of QA released by WT cells grown in copper-free SD supplemented with different concentrations of copper for 16 h. *F*, NAD$^+$ and NADH levels are slightly decreased by high copper stress. Results show WT cells grown in copper-free SD supplemented with different concentrations of copper for 16 h. *Error bars*, S.D. The *p* values are calculated using Student's *t* test (*, $p < 0.05$).

### *Mac1 and Hst1 co-repress de novo NAD$^+$ synthesis gene expression*

Mac1 is a copper-regulated transcription factor, which activates the expression of genes involved in high-affinity copper transport in response to copper deprivation (27–29). Our studies showed that deleting *MAC1* increases *de novo* NAD$^+$ synthesis activity and that the *mac1*Δ and *hst1*Δ mutants shared a similar effect on NAD$^+$ homeostasis (Fig. 2). To understand how Mac1 regulates NAD$^+$ metabolism, we carried out gene expression profile and differential gene expression studies in *mac1*Δ, *hst1*Δ, and WT cells (three biological triplicates of each strain were analyzed). A total of 370 genes were differentially

expressed in *mac1*Δ and WT cells (255 up-regulated, 115 down-regulated), and 498 genes were differentially expressed in *hst1*Δ and WT cells (342 up-regulated, 156 down-regulated) (Files S1 and S2). Gene ontology (GO) term enrichment analysis showed that *de novo* NAD$^+$ metabolism–associated GO terms were significantly enriched for the 498 differentially expressed genes in *hst1*Δ and WT cells. For the 370 differentially expressed genes in *mac1*Δ and WT cells, "copper ion import" and "iron ion homeostasis" GO terms were significantly enriched, which were in line with reported Mac1 function. In addition, "*de novo* NAD$^+$ biosynthetic process from tryptophan" and "quinolinate biosynthetic process" GO terms were also enriched, supporting a role for Mac1 in *de novo* NAD$^+$ metabolism. KEGG pathway mapping analysis also identified "tryptophan metabolism" as the most significantly enriched pathway (first, ranked by *p* values) in genes co-up-regulated by *mac1*Δ and *hst1*Δ. Consistent with these studies, expression of the *de novo* NAD$^+$ metabolism–associated *BNA* genes (*BNA1*, *-2*, *-4*, *-5*, and *-6*) was up-regulated in *hst1*Δ and *mac1*Δ cells (Fig. 3*A*, *left*). On the other hand, high-affinity copper transporter *CTR1* was specifically down-regulated in *mac1*Δ cells (Fig. 3*A*, *right*). These studies showed that in addition to being a transcription activator, Mac1 appeared to repress *BNA* gene expression.

Differential expression of additional NAD$^+$ homeostasis genes was also observed in *mac1*Δ and *hst1*Δ cells (Fig. 3*A*), including NAD$^+$ intermediate transporters *TNA1* and *NRT1*, and components of the phosphate-sensing *PHO* signaling pathway (26). Co-up-regulation of *TNA1* (NA and QA transporter) and *NRT1* (NR transporter) in *hst1*Δ and *mac1*Δ cells (Fig. 3*A*, *left*) was in line with the function of Hst1 as a NAD$^+$-regulated transcriptional repressor of NAD$^+$ homeostasis genes, and with the fact that *hst1*Δ and *mac1*Δ cells shared similar NAD$^+$ phenotypes. Expression of phosphatases (*PHO5*, *-11*, *-12*) and high-affinity phosphate transporter (*PHO84*) was increased in *hst1*Δ cells (Fig. 3*A*, *left*); however, it was either unchanged or decreased in *mac1*Δ cells (Fig. 3*A*, *right*). To further understand the roles of these factors in NAD$^+$ metabolism and to validate the expression profile results, we first carried out qPCR analysis in WT, *mac1*Δ, and *hst1*Δ cells. Fig. 3*B* showed that *mac1*Δ mutation increased *BNA* gene expression to a similar extent as seen in the *hst1*Δ mutant. The expression patterns of *BNA*, *PHO*, and *CTR1* genes were in agreement with expression profile analysis (Fig. 3, *A* and *B*). Next, we examined whether altered *PHO* gene expression indeed correlated with *PHO* signaling activities and whether it contributed to increased *de novo* NAD$^+$ synthesis. Previous studies associated *PHO* activation with increased NR and NA/NAM production (21, 26). We determined *PHO* activity by measuring the activity of *rAPase* (repressible acid phosphatase) Pho5, a periplasmic phosphatase activated by *PHO* signaling (35). As shown in Fig. 3*C*, *PHO* activity was moderately increased in the *hst1*Δ mutants but not in the *mac1*Δ mutant, which was consistent with observed *PHO* gene expression patterns (Fig. 3, *A* and *B*). Interestingly, observed *PHO* activation in *hst1*Δ cells appeared partially independent of the conventional *PHO* transcription factors Pho4-Pho2 complex, because deleting *PHO4* did not completely reduce *PHO* activation in *hst1*Δ cells. This study suggested that *PHO* activation is not essential for enhanced *de novo* NAD$^+$ synthesis in *mac1*Δ cells, and that Hst1 can activate specific *PHO* downstream targets independent of Pho4-Pho2.

It has been shown that during copper deprivation, Mac1 protein is stabilized and turns on copper homeostasis genes, including *CTR1*, whereas high copper concentrations facilitate the degradation of Mac1 (36, 37). Copper deprivation was also reported to induce *BNA* gene expression in strains defective in copper homeostasis (29, 38, 39). We therefore examined whether copper alterations would affect *BNA* gene expression in WT cells. As controls, expression of *CTR1* (Fig. 3*D*, *top right*) was induced by copper deprivation (0 $\mu$M), which was repressed by nutritional level (10 $\mu$M, normal) and a high level (250 $\mu$M) of copper. Interestingly, both low- and high-copper conditions appeared to induce the expression of a few *BNA* genes (Fig. 3*D*). Consistent with this, we showed that cells grown in media containing a nutritional copper level (10 $\mu$M) produced the lowest amount of QA and that both copper deprivation (0 $\mu$M) and high copper stress ($\geq$250 $\mu$M) increased QA production (Fig. 3*E*). High copper stress facilitates Mac1 degradation, which could explain the de-repression of *BNA* genes and QA production. However, copper might affect *BNA* gene expression independent of Mac1 because copper deprivation also moderately increased *BNA* gene expression and QA production. Interestingly, NAD$^+$ and NADH levels did not correlate with increased QA production under copper stress conditions (Fig. 3*F*). In fact, both NAD$^+$ and NADH levels were slightly reduced by high copper stress (Fig. 3*F*). It is possible that NAD$^+$ and its derivatives were consumed to offset the damages and redox changes caused by copper stresses. Together, these studies demonstrated a link between copper stress, *de novo* QA production, and NAD$^+$ metabolite homeostasis.

We next asked how might Mac1 and Hst1 co-repress *BNA* genes. Because *mac1*Δ and *hst1*Δ did not show a synergistic effect on NAD$^+$ homeostasis (Figs. 1*E* and 2 (*A*–*E*)), they likely function in a linear pathway to regulate *BNA* genes. As a transcription activator, Mac1 may activate *HST1* expression, which then represses *BNA* gene expression. This scenario was unlikely because expression of *HST1* was not altered in *mac1*Δ cells and vice versa (Fig. 3*B*). Mac1 has been shown to bind to the copper-response element (*CuRE*), TTTGC(TG)C(A/G) sequences, which are present in the promoters of copper homeostasis genes (40, 41). However, this consensus Mac1-binding motif is absent in the promoters of *BNA* genes. Hst1 and associated proteins have been reported to bind to the promoter of *BNA2* (42). We therefore examined whether Mac1 required Hst1 and vice versa to bind to the *BNA2* promoter. To address this question, ChIP studies of various *BNA2* promoter fragments using HA-tagged Hst1 (Hst1-HA) and Mac1 (Mac1-HA) were carried out. Fig. 4*A* (*top*) showed Mac1 and Hst1 protein levels in strains used for this study. Deleting *HST1* did not significantly alter Mac1 protein levels; likewise, deleting *MAC1* also did not alter Hst1 protein levels. Note that Mac1 was overexpressed for the ChIP studies because the Mac1 protein level was low and unstable in cells grown under nutritional levels of copper (standard conditions). Because all *mac1*Δ-associated NAD$^+$ homeostasis phenotypes were observed under standard conditions, we overexpressed Mac1 to enhance the sensitivity and to allow

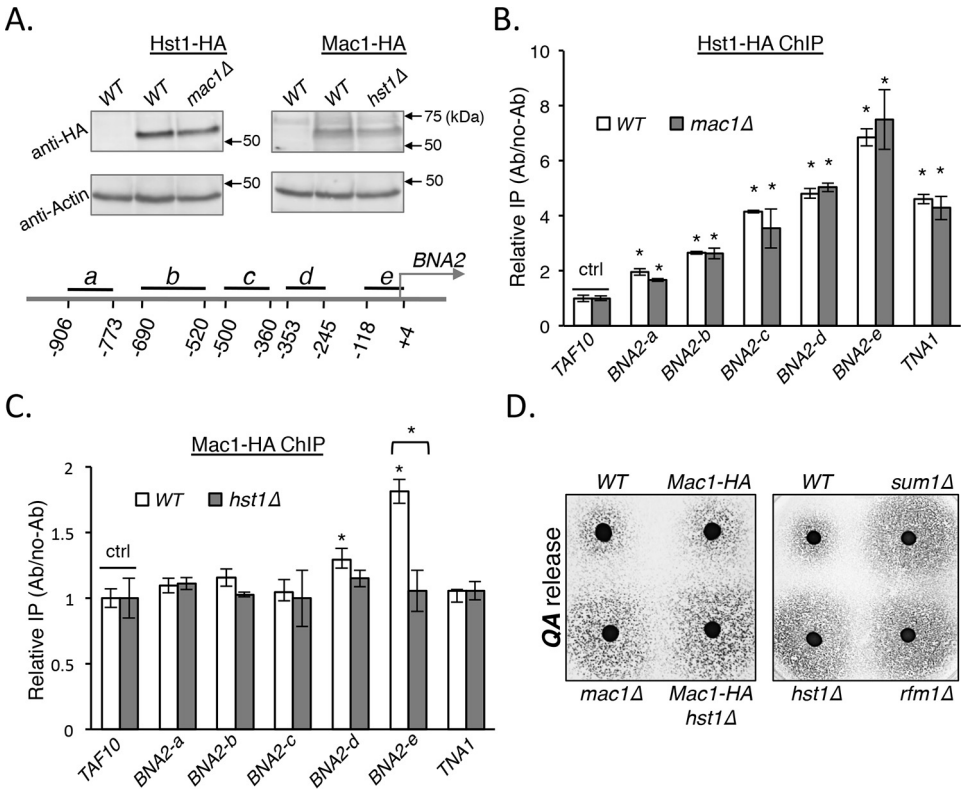


**Figure 4. Mac1 binds to the promoter of *BNA2* gene in an Hst1-dependent manner.** *A*, design of the ChIP studies. HA-tagged Hst1 was generated in both WT and *mac*1Δ cells. HA-tagged and overexpressed Mac1 was generated in WT and *hst1*Δ cells. Expression was confirmed via Western blot analysis (*top*). *BNA2* promoter regions for ChIP analysis are shown as *BNA2-a*, *BNA2-b*, *BNA2-c*, *BNA2-d*, and *BNA2-e* (*bottom*). *B*, Hst1 bound to the promoter regions of *BNA2* in both WT and *mac1*Δ cells with the highest binding activity near *BNA2-e*. Relative IP levels were normalized to *TAF10*. *TNA1* is a previously reported positive control. *C*, Mac1 showed the most significant binding to the *BNA2-e* region of the *BNA2* promoter in WT but not in cells lacking *HST1*. *D*, cells overexpressing HA-tagged *MAC1* show WT-level QA release (*left*). Mutants of the Hst1-Sum1-Rfm1 complex components show increased QA release (*right*). *Error bars*, S.D. The *p* values are calculated using Student's *t* test (*, $p < 0.05$).

further studies to be carried out under normal copper conditions. Fig. 4*A* (*bottom*) illustrates *BNA2* promoter fragments (*BNA2-a*, *-b*, *-c*, *-d*, and *-e*) examined in ChIP studies. As shown in Fig. 4*B*, Hst1 was bound to all five *BNA*2 promoter fragments, with the most significant binding activity near the *BNA2-e* region. Deleting *MAC1* did not significantly alter Hst1 binding to *BNA2* promoter fragments, indicating that Hst1 did not require Mac1 to bind to *BNA2* promoter (Fig. 4*B*). On the other hand, Mac1 only showed significant binding near the *BNA2-e* region (Fig. 4*C*). Interestingly, Mac1 binding to the *BNA2-e* region was abolished in *hst1*Δ cells, indicating that Hst1 is essential for Mac1 binding. It remained possible that Mac1 also bound to other regions of the *BNA2* promoter; however, our assay conditions were not sensitive enough to detect the binding. It was also likely that the Mac1 overexpression might hinder its binding activity. This was less likely because cells overexpressing Mac1 still showed normal QA release (Fig. 4*D*, *left*), indicating that overexpression did not significantly affect Mac1 function at *BNA* promoters. Among Hst1-associated protein complexes, the Hst1-Sum1-Rfm1 complex appeared to play a key role in *BNA* repression because both *sum1*Δ and *rfm1*Δ mutants were also identified in our screen and showed increased QA release (Fig. 4*D*, *right*). Overall, these studies suggested that Mac1 works with the Hst1-associated repressor complex to regulate *BNA* genes, and deleting *MAC1* or *HST1* alone is sufficient to abolish the repression.

### *Regulation of de novo NAD$^+$ synthesis by NA salvage*

An unexpected phenomenon was observed while developing the QA cross-feeding reporter system, which indicated that *de novo* NAD$^+$ synthesis is also regulated by an Hst1/Mac1-independent mechanism. In the reporter system, QA released by the feeder cells (mutants of interest) supported the growth of the QA-dependent recipient cells (readout for QA release). When grown on standard rich medium YPD, all strains tested, including the *hst1*Δ and *mac1*Δ mutants, appeared to be defective in QA production and failed to support the recipient cell growth (Fig. 5*A*, *panel 1*). On the other hand, cells grown on minimal synthetic medium SD were able to produce QA in an Hst1- and Mac1-regulated manner (Fig. 5*A*, *panel 2*). NA was shown to repress *de novo* NAD$^+$ synthesis, and the amount of NA differed significantly in standard SD (0.4 mg/liter, ~3.3 $\mu$M) and YPD (~13–61 mg/liter, ~100–500 $\mu$M). However, NA-mediated repression was suggested to require NA salvage into NAD$^+$ and NAD$^+$-dependent activation of Hst1 (30). These observations prompted us to examine whether NA played a role in this seemingly Hst1/Mac1-independent repression. As shown in Fig. 5*A* (*panels 2–5*), QA levels released by WT, *mac1*Δ, and *hst1*Δ cells indeed inversely correlated with NA levels (0 mg/liter, NA-free SD; 0.4 mg/liter, SD/normal; ≥61 mg/liter, high NA) in growth media. In contrast, NAM enhanced QA release, and it did not further increase QA release

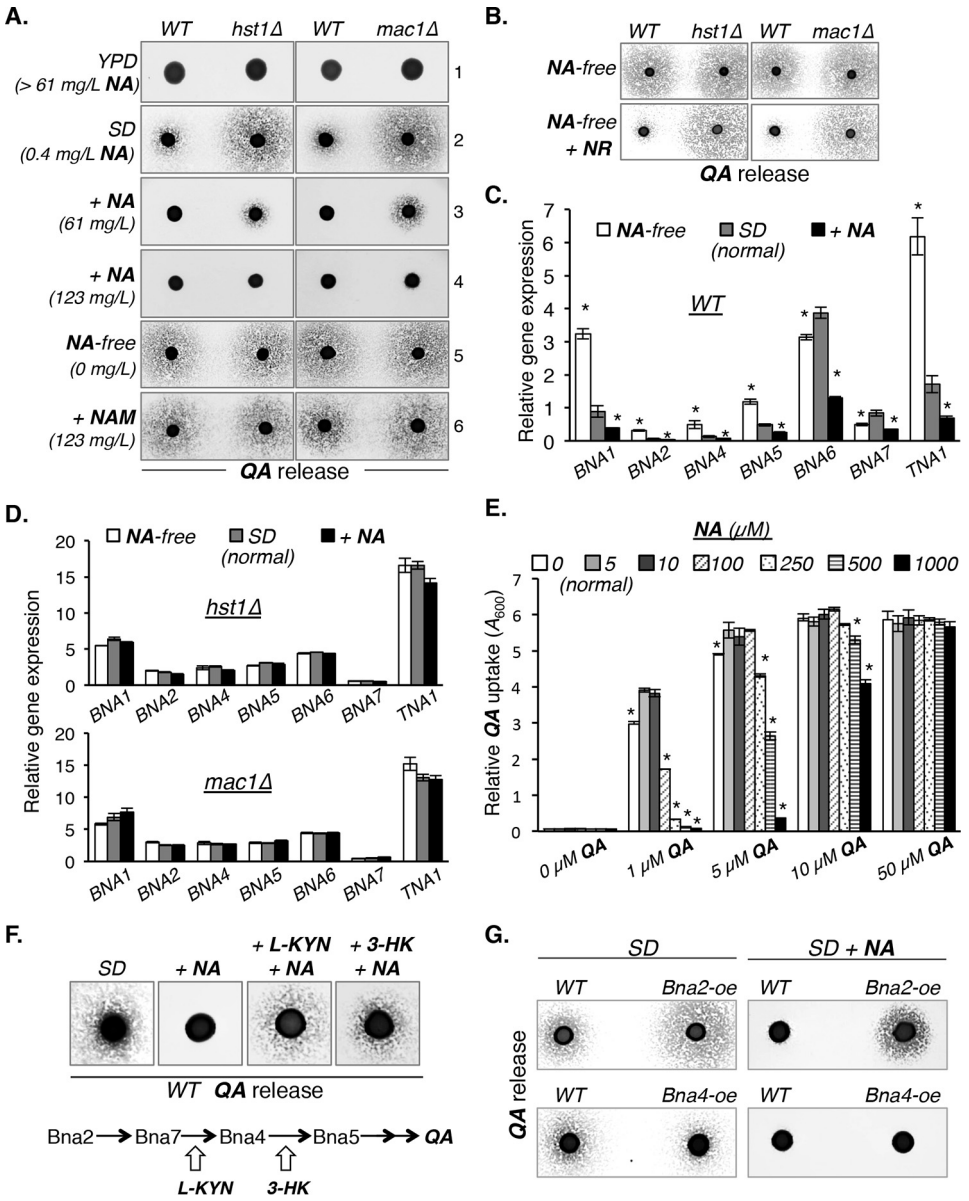


**Figure 5. NA inhibits the activity of the *de novo* pathway.** *A*, levels of QA production inversely correlate with the concentrations of NA present in the growth media. Results show released QA levels in WT, *hst1*Δ, and *mac1*Δ cells grown in the following media: YPD, NA-free SD, SD (*normal*), and SD supplemented with NA (+*NA*) or NAM (+*NAM*). NAM is a competitive inhibitor of the NAD$^+$-dependent deacetylases. *B*, NA inhibits QA production in an NAD$^+$/Hst1-dependent manner. Elevated QA release in WT cells grown in NA-free media was rescued by restoring NAD$^+$ levels via supplementing NR (at 20 μM, a NAD$^+$ precursor). Hst1 was required for the rescue. *C*, most *BNA* gene expression in WT cells shows an inverse correlation with NA levels in growth media. Cells were grown in NA-free, SD (*normal*) and +NA (at 123 mg/liter) media. Relative gene expression determined by qPCR (normalized to *TAF10*) is shown. *D*, *BNA* gene expression in *hst1*Δ and *mac1*Δ cells is not altered by NA levels. Cells were grown in NA-free, SD (*normal*), and +NA (at 123 mg/liter) media. Relative gene expression determined by qPCR (normalized to *TAF10*) is shown. *E*, QA uptake is inhibited by NA in a dose-dependent manner, which is alleviated by increasing QA concentrations. The QA-dependent *npt1*Δ*nrk1*Δ*bna4*Δ mutant was grown in SD containing different levels of QA and NA. The extent of growth ($A_{600}$) of this mutant correlates with its QA uptake efficiency. *F*, NA-mediated inhibition of QA production can be rescued by supplementing specific intermediates of the *de novo* pathway. Results show relative QA production in WT cells grown in SD supplemented with NA (40 mg/liter) and L-Kyn (1 mM) or 3-HK (0.25 mM). *G*, *BNA2* overexpression (*Bna2-oe*) restores QA release in WT cells grown in SD supplemented with NA (20 mg/liter). *Error bars*, S.D. The *p* values are calculated using Student's *t* test (*, $p < 0.05$).

in *hst1*Δ and *mac1*Δ cells (Fig. 5*A*, *panel 6*). Although NAM can be deamidated into NA, it also inhibits the activity of the Sir2 family deacetylases (43, 44). Therefore, NAM was anticipated to induce *hst1*Δ-like phenotypes. These results indicated that high NA–mediated inhibition of QA production did not require Hst1 and Mac1 (Fig. 5*A*, *panels 2–4*). However, elevated QA release observed in WT cells grown in NA-free media could be rescued by restoring NAD$^+$ levels via supplementing NR (Fig. 5*B*), and that NR-mediated rescue required functional *HST1* (Fig. 5*B*). Thus, it appeared that NA could inhibit *de novo* pathway activity in both an NAD$^+$/Hst1-dependent (Fig. 5*B*) and an NAD$^+$/Hst1-independent manner (Fig. 5*A*), depending on the NA levels in growth media.

Interestingly, NA-induced inhibitions were not completely due to repression of *BNA* genes. In WT cells, the expression of most *BNA* genes inversely correlated with the levels of NA in growth media (Fig. 5*C*). However, in *hst1*Δ and *mac1*Δ cells, elevated *BNA* expression was not altered by NA treatments

(Fig. 5*D*), indicating that *mac*Δ and *hst1*Δ cells still produced elevated levels of QA regardless of NA levels. This suggested that high NA might actually hinder growth of the QA-dependent recipient cells, masking the QA cross-feeding readout (Fig. 5*A*, *panels 1*, *3*, and *4*). The NA transporter Tna1 has been reported to also transport QA (22). It was shown that the *tna1*Δ mutant failed to transport QA (1–3.3 $\mu$M) and thus exhibited growth defects in NA-free media under anaerobic conditions in which the *de novo* NAD$^+$ pathway is completely blocked and the cells depend on QA transport for growth (22). Because Tna1 can transport both NA and QA, it is possible that high NA competes with QA for Tna1-mediated transport. To address this, we examined whether high NA could inhibit QA uptake by exploiting the QA-dependent *npt1*Δ*nrk1*Δ*bna4*Δ recipient cell mutant. This mutant cannot utilize NA (due to *npt1*Δ mutation); therefore, its *de novo* pathway gene expression is not altered by NA treatments. As a result, the extent of cell growth ($A_{600}$) of this mutant in media containing different levels of QA and NA correlates with its QA uptake efficiency. As shown in Fig. 5*E*, NA indeed inhibited QA uptake in a dose-dependent manner. At 5–10 $\mu$M NA (approximate NA levels in SD), no inhibition of QA uptake was observed. High NA ($\geq$100 $\mu$M) showed the most significant inhibition of QA uptake when QA was supplemented at 1–5 $\mu$M, which was similar to reported QA levels released by WT cells in SD (22). Observed NA inhibitions of QA uptake could be alleviated by increasing QA concentrations (at 10–50 $\mu$M) (Fig. 5*E*), suggesting that NA competes with QA for Tna1-mediated transport. It remains possible that NA may also inhibit intracellular QA utilization. One possible target is the enzymatic activity of Bna6, a quinolinate phosphoribosyl transferase (QPRT) that converts QA into NaMN (Fig. 1*A*). However, it has been shown that NA does not inhibit QPRT activity (45, 46). Together, these results suggested that high NA could also inhibit the *de novo* pathway activity by competing with QA transport, which is independent of NA salvage into NAD$^+$ and Hst1-mediated *BNA* gene repression.

Nevertheless, Hst1-mediated *BNA* gene repression remains the major mechanism of NA/NAD$^+$-induced inhibition of *de novo* QA/NAD$^+$ synthesis. To further understand this regulation, we first determined which *BNA* gene was most sensitive to NA inhibition using QA production as readout. A simplified *de novo* QA production pathway was illustrated in the *bottom panel* of Fig. 5*F*. The QA-dependent *npt1*Δ*nrk1*Δ*bna1*Δ mutant was used as the recipient cells whose growth correlates with the levels of QA released by the WT donor cells. As shown in Fig. 5*F* (*top*), levels of QA released by WT donor cells were inhibited by NA (at $\leq$40 mg/liter NA to minimize its inhibition of QA uptake). This inhibition could be rescued by supplementing L-KYN or 3-HK (Fig. 5*F*, *top*) suggesting that the expression of *BNA2* or *BNA7* in the WT donor cells was most sensitive to NA-induced Hst1-mediated repression (Fig. 5*F*, *bottom*). Because *BNA7* expression appeared less sensitive to NA alterations (Fig. 5*C*) and *hst1*Δ mutation (Fig. 5*D*), we directly examined *BNA2.* As shown in Fig. 5*G*, overexpressing *BNA2* was sufficient to increase QA release (*left*) and rescue NA inhibition (*right*) in WT cells. As controls, overexpressing *BNA4* did not show significant effects on QA release. These results indicate that *BNA2* expression is most sensitive to Hst1- and NA-mediated repression, and therefore it is likely a rate-limiting step in *de novo* QA production.

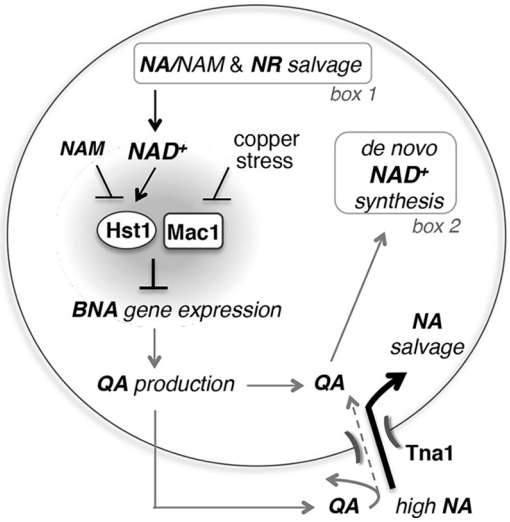


**Figure 6. A model depicting the regulation of QA production and the *de novo* pathway activity by NA/NAD$^+$-dependent Hst1, copper-regulated Mac1, and NA-inhibited QA transport.** NAD$^+$ can be synthesized *de novo* from tryptophan via the *BNA* proteins (*box 2*) or salvaged from intermediates and small precursors such as NA, NAM, and NR (*box 1*). For clarity, this diagram centers on the regulation of the *de novo* pathway (*shaded area*). Under NA-abundant conditions, NA/NAM salvage is the preferred NAD$^+$ biosynthesis route, and *BNA* genes are silenced by the NAD$^+$-dependent Hst1. NAM can be deamidated into NA and contributes to NAD$^+$ biosynthesis, but it also inhibits Hst1 activity. The copper-sensing transcription factor Mac1 appears to work in concert with the Hst1-containing repressor complex to repress *BNA* genes. Yeast cells also release and re-uptake small NAD$^+$ precursors, such as NA, NAM, NR, and QA; however, the mechanisms are not completely understood. It has been suggested that vesicular trafficking and vacuolar function play a role in the production and release of NAD$^+$ precursors. Uptake of NAD$^+$ precursors is mostly mediated by specific transporters, including Nrt1 (for NR) and Tna1 (for NA and QA). High levels of NA in the growth media hinder the re-uptake of released QA, thereby reducing the *de novo* activity.

## Discussion

In this study, we identified Mac1 as a novel NAD$^+$ homeostasis factor in yeast. Mac1 was previously characterized as a copper-sensing transcription activator (27–29). Cells lacking *MAC1* shared similar NAD$^+$ phenotypes with the *hst1*Δ mutant. The NAD$^+$-dependent histone deacetylase Hst1 has been suggested to be an NAD$^+$ sensor, which inhibits *de novo* NAD$^+$ synthesis by repressing *BNA* gene expression when NAD$^+$ is abundant (Fig. 6) (30). We showed that deleting either *MAC1* or *HST1* was sufficient to abolish *BNA* gene repression (Fig. 3, *A* and *B*). Although *BNA* gene promoters lack Mac1-binding sequences *CuRE*, Mac1 proteins likely associate with *BNA* promoters with help from the Hst1 complex (Fig. 4*C*). On the other hand, Hst1 binding to the *BNA2* promoter does not require functional Mac1 (Fig. 4*B*), indicating that binding of the Hst1 complex precedes Mac1 at the *BNA2* promoter. Together, these results suggest that Mac1 proteins work with the Hst1-containing repressor complexes (Hst1, Rfm1, and Sum1) formed at the *BNA* promoters to repress gene expression. It remains unclear how Mac1 proteins work with the Hst1 complexes to mediate *BNA* gene repression. Although Mac1 and Hst1 complex components did not appear to directly interact in systematic pulldown studies (47, 48), they may interact under

specific conditions. Mac1 and Sum1 were reported to share a common interacting partner, histone H4 (Hhf1) (47, 48), suggesting a possible interaction model. Interestingly, both Mac1 and Hst1 proteins showed higher binding activities at the *BNA2* promoter regions near the start codon (Fig. 4, *B* and *C*), suggesting that Mac1 and Hst1 binding to these regions is more critical for *BNA2* gene repression. Further studies are required to understand how Mac1 contributes to Hst1-mediated *BNA* gene repression.

Our studies also uncovered additional NA-mediated regulation of the *de novo* pathway. The NAD$^+$ pool is maintained by NA and NR salvage pathways and *de novo* NAD$^+$ synthesis from tryptophan (Fig. 6). Under NA-abundant conditions, NA salvage is the preferred NAD$^+$ synthesis route (30, 34), which leads to Hst1 activation and *BNA* gene repression. As cells consume NA, eventually NA/NAD$^+$ deprivation decreases Hst1 activity, leading to de-repression of *BNA* genes, QA production, and *de novo* NAD$^+$ synthesis. Supporting this, cells grown in NA-free media showed increased *BNA* gene expression (Fig. 5*C*) and QA production (Fig. 5*A*). Supplementing NR to NA/NAD$^+$-deprived cells was sufficient to restore their NAD$^+$ levels and repression of QA production (Fig. 5*B*). It appears that QA production occurs before complete depletion of NA/NAD$^+$ because QA release is detectable in log-phase WT cell culture, which is further increased in stationary phase culture (22). Most excess QA (if not converted to NAD$^+$) is released extracellularly (Fig. 2*A*) and can re-enter cells via Tna1 (also a high-affinity NA transporter) (22) as the NA levels decline. Supporting this, the high QA–producing *hst1*Δ and *mac1*Δ mutants showed more significant increases in NAD$^+$ levels when NA was depleted in the growth media (Fig. 2, *E* and *F*). Thus, NA inhibits *de novo* NAD$^+$ synthesis both by repressing QA production (Fig. 5, *B* and *C*) and by competing with QA transport (Fig. 5*E*); the latter is particularly significant when cells are grown in rich media, which contain high levels of NA (~100–500 $\mu$M) (Fig. 5*A*, *panel 1*). We have also shown *BNA2* expression is most sensitive to NA-mediated repression (Fig. 5*F*), and *BNA2* is a rate-limiting step in QA production (Fig. 5*G*). Overall, these studies provide further understanding of the dynamic interactions between NA salvage and *de novo* NAD$^+$ synthesis.

Additional nutritional stresses also play a role in regulating *de novo* NAD$^+$ synthesis. Copper has been shown to negatively regulate Mac1-dependent transcription activation. Under copper deprivation, Mac1 remains stable and activates expression of genes in the high-affinity copper transport system (36, 37, 49). Upon copper repletion, copper binding to Mac1 causes an intramolecular interaction between its N-terminal DNA binding domain and C-terminal trans-activating domain, resulting in a transcriptionally inactive state. Under high-copper conditions, Mac1 is quickly degraded to avoid copper toxicity (36, 37, 49). Thus, the copper-bound form of Mac1, although transcriptionally inactive, is likely to bind to and repress *BNA* gene promoters because our studies were carried out under nutritional copper levels. High copper stress caused Mac1 degradation (36, 37, 49), which was in line with increased *BNA* gene expression (Fig. 3*D*) and QA production (Fig. 3*E*). Interestingly, copper deprivation also increased *BNA* expression (Fig. 3*D*) and QA production (Fig. 3*E*). It is possible that the transcriptionally active form of Mac1 binds to *CuRE* promoters more efficiently than to the *BNA* promoters during copper deprivation. Alternatively, copper may regulate *BNA* gene expression independent of Mac1. Together, these studies demonstrate that a dynamic Mac1 pool is shared between the Hst1-containing repressor complexes at *BNA* promoters and the transcription-activating complexes at *CuRE*-containing promoters. However, NAD$^+$ levels did not appear to correlate with increased QA production under copper stress conditions (Fig. 3*F*). It is likely that NAD$^+$ is consumed or converted to NAD$^+$ derivatives, such as NADH, NADP$^+$, and NADPH, to maintain proper redox state and to prevent and counteract copper stress-induced oxidative damages. In addition, copper may inhibit the activities of NAD$^+$ metabolic enzymes. For example, copper was shown to inhibit the activity of QPRT (50, 51). It is also possible that under stress conditions, it is beneficial for cells not to increase NAD$^+$ levels to maintain an optimal metabolic state.

It appears that once QA is produced from *de novo* synthesis, it is either released to the extracellular environment or converted to NAD$^+$ (Fig. 6). In yeast, released QA can re-enter cells to support NAD$^+$ synthesis via the NA transporter (22). Yeast cells also release and re-uptake other small NAD$^+$ precursors that arise from NA/NAM salvage and NR salvage, such as NA, NAM, and NR (1, 21, 52). It has been suggested that vesicular trafficking and vacuolar function play a role in the production and release of these NAD$^+$ precursors (1, 21, 52). However, the detailed mechanisms are not completely understood. There appears to be a storage pool for NAD$^+$ precursors generated from the salvage pathways. For example, cytoplasmic NR is released to the environment or transported into the vacuole for storage if not converted to NAD$^+$. Likewise, vacuolar NR may exit the vacuole to support NAD$^+$ synthesis in the cytoplasm. The equilibrative nucleoside transporter Fun26 (human lysosomal hENT homolog) controls the balance of NR and possibly other nucleosides between the vacuole and the cytoplasm (26). It is possible that vacuolar degradation of NAD$^+$ intermediates coincides with NAD$^+$ salvage. NAD$^+$ intermediates may enter the vacuole through vesicular transport and autophagy and are then broken down into smaller precursors for storage or reuse. On the other hand, when excess QA is made in the cytoplasm, it is mostly released and not stored in the vacuole. Interestingly, the *fun26*Δ mutant showed increased QA production/release (Table S1). This is likely due to the blockage of NR salvage–mediated NAD$^+$ synthesis because NR is trapped inside the vacuole in the *fun26*Δ mutant. We have shown that NAD$^+$ depletion causes *BNA* gene de-repression and that NR supplementation restores the repression in an Hst1-dependent manner (Fig. 5*B*). In line with this, cells lacking the NAM deamidase *PNC1* also showed increased QA production (Table S1). The *pnc1*Δ mutation causes accumulation of NAM (21), which is anticipated to inhibit Hst1 activity. Therefore, increased QA production observed in the *fun26*Δ and *pnc1*Δ mutants was likely due to loss of Hst1-mediated repression of *BNA* genes. Together, these studies demonstrate a complex interconnection between the *de novo* and salvage pathways.

In summary, our studies have uncovered novel NAD$^+$ homeostasis factors. Hst1 and Mac1 may play important roles in the cross-regulation of *de novo* NAD$^+$ synthesis and other nutrient-sensing pathways. Copper levels determine the conformation and stability of the Mac1 proteins, resulting in corresponding changes in *de novo* QA production and copper homeostasis. In addition, increased phosphate-sensing *PHO* activity was also observed in the *hst1*Δ mutant. Activation of *PHO* has been associated with increased NR (26) and NA/NAM (21) production, suggesting that Hst1 may also affect NR and NA/NAM salvage activities via regulating specific components in the *PHO* pathway. Recent studies have demonstrated that NAD$^+$ metabolism is a therapeutic target for several human diseases. This strategy was more effective when specific defects in NAD$^+$ biosynthesis were identified and associated with the progression of diseases (9, 10). Supplementation of specific NAD$^+$ precursors can also be combined with the use of genetic modifications and inhibitors of specific NAD$^+$ biosynthesis steps to help channel the precursors' flow through a more efficient NAD$^+$ synthesis route (9, 53, 54). Recent studies have also shown that inhibiting the activities of *de novo* pathway enzymes, such as tryptophan 2,3-dioxygenase (TDO; Bna2 in yeast) (55) and kynurenine 3-monooxygen (KMO; Bna4 in yeast) (56), as well as increasing the ratio of neuroprotective KA over neurotoxic QA or 3-HK, may help to alleviate a few neurological disorders (24, 55). Understanding the molecular basis and interconnection of multiple NAD$^+$ metabolic pathways is important for the development of disease-specific therapeutic strategies. Overall, our studies contribute to the understanding of the regulation of NAD$^+$ metabolic pathways and may provide insights into the underlying mechanisms of disorders associated with aberrant NAD$^+$ metabolism.

## Experimental procedures

### *Yeast strains, growth media, and plasmids*

Yeast strain BY4742 *MATα his3Δ1 leu2Δ0 lys2Δ0 ura3Δ0* was acquired from Open Biosystems (57). Standard media, including yeast extract-peptone-dextrose (YPD), SD, and SC media were made as described (58). NA-free SD and NA-free SC were made by using niacin-free yeast nitrogen base (Sunrise Science Products). Single gene deletion mutants were generated by replacing the WT genes with a reusable *loxP-kanMX-loxP* cassette as described (59). Making mutants with multiple gene deletions employed a galactose-inducible Cre recombinase to remove the reusable *loxP-kanMX-loxP* cassette, followed by another round of gene deletion (59). In strains carrying nonreusable *kan* markers, gene deletion was introduced by using a hygromycin resistance marker (pAG32-hphMX4) (60). The HA epitope tag was added to target genes directly in the genome using the pFA6a-3HA-kanMX6 (*HST1*) or pFA6a-kanMX6-PGAL1–3HA (*MAC1*) plasmids as template for PCR-mediated tagging (61). The *BNA2* and *BNA4* overexpression plasmids, p*ADH1-BNA2* and p*ADH1-BNA4*, were made in the integrative pPP81 (*LEU2*) vector and were introduced to yeast cells as described (62).

### *QA cross-feeding spot assays*

The *npt1*Δ*nrk1*Δ*bna1*Δ and *npt1*Δ*nrk1*Δ*bna4*Δ mutants (which depend on QA for growth) were used as "recipient cells," and yeast strains of interest were used as "feeder cells." First, recipient cells were plated onto SD as a lawn (~$10^4$ cells/cm$^2$). Next, ~$2 \times 10^4$ cells of each feeder cell strain (2 μl of cell suspension made in sterile water at $A_{600}$ of 1) were spotted onto the lawn of recipient cells. Plates were then incubated at 30 °C for 3 days. The extent of the recipient cell growth indicates the levels of QA released by feeder cells.

### *Genetic screen using the yeast deletion collection*

The haploid yeast deletion collection (~4,500 strains) established in the BY4742 strain was acquired from Open Biosystems (63). To screen for mutants with altered QA release, 2 μl of each strain was directly taken from the frozen stock and then spotted onto SD plates spread with the *npt1*Δ*nrk1*Δ*bna4*Δ recipient cells at a density of ~$10^4$ cells/cm$^2$. After incubation at 30 °C for 3 days, we scored the cross-feeding activity (which indicates the level of QA release) of each mutant by comparing the diameter of the cross-feeding zones with that of the WT. Mutants were assigned a score of −4 through 4 (WT = 0). Scores of −4, −3, and −2 indicate decreased QA release; scores of +2, +3, and +4 indicate increased QA release. To eliminate false-positives, mutants with scores of −4, −3, 3, and 4 (169 mutants) were re-examined. A total of 81 mutants passed the secondary screen on both SD and SC growth media (Table S1).

### *Measurement(s) of NAD$^+$, NADH, QA, NR, and NA/NAM*

Total intracellular levels of NAD$^+$ and NADH were determined using enzymatic cycling reactions as described (62). Levels of NAD$^+$ intermediates (QA, NR, and NA/NAM) were determined by a liquid-based cross-feeding bioassay as described previously (20, 21, 26) with modifications. To prepare cell extracts for intracellular NAD$^+$ intermediates determination, ~150 $A_{600}$ unit (1 $A_{600}$ unit = $1 \times 10^7$ cells/ml) donor cells grown to late logarithmic phase in SC (~16 h of growth from an $A_{600}$ of 0.1) were collected by centrifugation and lysed by bead-beating (Biospec Products) in 800 μl of ice-cold 50 mM ammonium acetate solution. After filter sterilization, 100 μl of clear extract was used to supplement 8-ml cultures of recipient cells with starting $A_{600}$ of 0.05 in SC. To determine extracellular NAD$^+$ intermediates levels, supernatant of donor cell culture was collected and filter-sterilized, and then 500 μl was added to 7.5 ml of recipient cell culture with total starting $A_{600}$ of 0.05 in SC. A control culture of recipient cells in SC without supplementation was included in all experiments. For measuring relative QA levels, *npt1*Δ*nrk1*Δ*bna4*Δ and *npt1*Δ*nrk1*Δ*bna1*Δ mutants were used as recipient cells. The *npt1*Δ*bna6*Δ*pho5*Δ recipient cells were used to measure relative NR levels. To measure relative NA/NAM levels, the *bna6*Δ*nrk1*Δ*nrt1*Δ recipient cells were grown in NA-free SC. After incubation at 30 °C for 24 h, growth of the recipient cells ($A_{600}$) was measured and normalized to the cell number of each donor strain. $A_{600}$ readings were then converted to concentrations of QA, NR, and NA/NAM using the standard curves established as described previously (Fig. S1) (20, 21).

### *Gene expression profile analysis*

Approximately 40 $A_{600}$ unit cells grown to early logarithmic phase in SD (6-h growth from an $A_{600}$ of 0.1) were collected by centrifugation. Total RNA was extracted using the GeneJET RNA purification Kit (Thermo Scientific). High-quality DNA-free RNA for sequencing was made using the RNA Clean and Concentrator kit (Zymo Research). For each sample, 10 $\mu$l of RNA (at 100 ng/$\mu$l) was used to generate 3′-Tag-Seq libraries (a single initial library molecule per transcript, complementary to 3′-end sequences, was generated). The libraries were then sequenced by single-end sequencing on the HiSeq 4000 (DNA Technology Core, University of California, Davis, CA). Three biological triplicates of each strain were sequenced. Differential gene expression testing was conducted using a single-factor analysis of variance model in the limma-voom Bioconductor pipeline (Bioinformatics Core, University of California, Davis, CA). Prior to analysis, genes with expression less than 1 count per million reads were filtered, leaving 6,023 of 7,126 genes. The multidimensional scaling plot shows the distance between samples based only on normalized counts. In this experiment, the WT samples clustered together and were very different than the mutants, as expected. GO enrichment analyses of differential gene expression results were conducted using Kolmogorov–Smirnov tests in the Bioconductor package topGO. For each GO term, the KS test tests whether *p* values for genes annotated with that GO term are smaller than for genes not annotated with that GO term. KEGG enrichment analyses were conducted using Wilcoxon rank sum tests, in conjunction with the Bioconductor package KEGGREST. For each KEGG pathway, the Wilcoxon rank-sum test tests whether *p* values for genes in that pathway are smaller than genes not in that pathway. Enrichment analyses of genes that are significantly up or significantly down in both *mac1*Δ and *hst1*Δ mutants relative to WT were obtained by KEGG and GO enrichment analyses of gene lists from Venn diagrams. Fisher's exact test was used to test whether the number of genes in the Venn list in a given pathway/GO term was greater than would be expected by chance.

### *Quantitative PCR (qPCR) analysis of gene expression levels*

Approximately 40 $A_{600}$ unit cells grown to early logarithmic phase in SD (6 h of growth from $A_{600}$ of 0.1) were collected by centrifugation. Total RNA was isolated using the GeneJET RNA purification Kit (Thermo Scientific), and cDNA was synthesized using the QuantiTect reverse transcription kit (Qiagen) according to the manufacturer's instructions. For each qPCR, 50 ng of cDNA and 500 nM each primer were used. The qPCR was run on a Roche LightCycler 480 using LightCycler 480 SYBR Green I Master Mix (Roche Applied Science) as described previously (64). The average size of the amplicon for each gene was ~150 bp. The target mRNA transcript levels were normalized to *TAF10* transcript levels.

### *rAPase activity assay*

The *rAPase* liquid assay was carried out as described (35) using cells grown to late log phase in SC. In brief, 2.5 $A_{600}$ unit cells were harvested, washed, and resuspended in 150 $\mu$l of water. Next, 600 $\mu$l of substrate solution (5.6 mg/ml *p*-nitrophenylphosphate in 0.1 M sodium acetate, pH 4) was added to cell suspension, and the mixture was incubated at 30 °C for 15 min. The reaction was stopped by adding 600 $\mu$l of ice-cold 10% TCA. 600 $\mu$l of this final mixture was then added to 600 $\mu$l of saturated $Na_2CO_3$ to allow color (neon yellow) development. Cells were pelleted to acquire the supernatant for $A_{420}$ determination. The *rAPase* activities were determined by normalizing $A_{420}$ readings to total cell number ($A_{600}$).

### *Protein extraction and Western blot analysis*

A total of 100 ml of cells were grown in SD to early logarithmic phase ($A_{600}$ of ~1) and collected by centrifugation. The cell lysate was obtained by bead-beating in lysis buffer (50 mM Tris-HCl, pH 7.5, 100 mM NaCl, 1% Nonidet P-40 (Sigma), and protease inhibitor mixture (Pierce™). The protein concentration was measured using the Bradford assay (Bio-Rad), and 30 $\mu$g of total protein was loaded in each lane. After electrophoresis, the protein was transferred to a nitrocellulose membrane (Amersham Biosciences™ Protran™, GE Healthcare). The membranes were then washed and blotted with either anti-HA antibody (Invitrogen) or anti-$\beta$-actin antibody (Abcam). Protein was visualized using anti-mouse IgG antibody conjugate to the horseradish peroxidase (GE Healthcare) and the ECL reagents (Amersham Biosciences™, GE Healthcare). The chemiluminescent image was analyzed using the Amersham Biosciences Imager 600 (GE Healthcare) system and software provided by the manufacturer.

### *ChIP assay*

Approximately 500 $A_{600}$ unit cells grown to early logarithmic phase in SD were cross-linked with 1% formaldehyde for 30 min at room temperature and stopped by adding glycine to a final concentration of 125 mM. Cells were pelleted by centrifugation and washed two times with cold TBS (20 mM Tris-HCl, pH 7.5, 150 mM NaCl). Cells were lysed by bead beating in 1 ml of FA-140 lysis buffer (50 mM HEPES, 140 mM NaCl, 1% Triton X-100, 1 mM EDTA, 0.1% sodium deoxycholate, 0.1 mM PMSF, 1× protease inhibitor mixture (Pierce)) (33). The cell lysate was drawn off the beads and centrifuged at a maximum speed (13,200 rpm) for 30 min at 4 °C. The chromatin pellet was resuspended in 1 ml of FA-140 lysis buffer and sonicated on ice eight times with 20-s pulses using a Branson 450 Sonicator (output control set at 1.5 and duty cycle held at constant) to shear chromatin to an average length of ~500 bp. Sonicated chromatin solution was centrifuged twice at 10,000 rpm for 10 min at 4 °C. The supernatant was then aliquoted into three tubes (labeled "input," "IP," and "no-Ab"). The IP samples were incubated overnight at 4 °C with anti-HA mAb (ab1424, Abcam) at a dilution of 1:150. Both IP and no-Ab samples were incubated with 60 $\mu$l of ChIP-grade protein G beads (Cell Signaling Technology) for 2 h at 4 °C and then washed as described (33). DNA was then eluted from the beads two times with 125 $\mu$l of elution buffer (50 mM Tris-HCl, pH 8, 10 mM EDTA, 1% SDS). The combined DNA solution and input samples were incubated at 65 °C overnight to reverse the cross-linking. The purified DNA samples were analyzed by qPCR, and results were compared with a standard curve prepared from input DNA. The amount of immunoprecipitated specific promoter DNA

was determined relative to no-Ab DNA. S.D. values were calculated from the results of three independent biological replicates.

*Author contributions*—C. J. T. R. and S.-J. L. conceptualization; C. J. T. R., G. D., T. Cater, and S.-J. L. data curation; C. J. T. R. and T. Croft formal analysis; C. J. T. R., T. Croft, B. G., and G. D. validation; C. J. T. R., T. Croft, P. V., B. G., G. D., and T. Cater investigation; C. J. T. R., T. Croft, P. V., B. G., and S.-J. L. visualization; C. J. T. R., T. Croft, P. V., and B. G. methodology; C. J. T. R. and S.-J. L. writing-original draft; C. J. T. R., T. Croft, P. V., B. G., and S.-J. L. writing-review and editing; S.-J. L. supervision; S.-J. L. funding acquisition; S.-J. L. project administration.

*Acknowledgments—We thank Dr. M. L. Settles and Dr. M. Britton (Genome Center and Bioinformatics Core Facility) for assistance with RNA Tag-Seq data analysis and Dr. J. Roth and Dr. S. Collins for suggestions and discussions.*

## References


1. Kato, M., and Lin, S. J. (2014) Regulation of NAD$^+$ metabolism, signaling and compartmentalization in the yeast Saccharomyces cerevisiae. *DNA Repair* **23,** 49–58 CrossRef Medline
2. Nikiforov, A., Kulikova, V., and Ziegler, M. (2015) The human NAD metabolome: functions, metabolism and compartmentalization. *Crit. Rev. Biochem. Mol. Biol.* **50,** 284–297 CrossRef Medline
3. Chini, C. C. S., Tarragó, M. G., and Chini, E. N. (2017) NAD and the aging process: role in life, death and everything in between. *Mol. Cell. Endocrinol.* **455,** 62–74 CrossRef Medline
4. Imai, S., and Guarente, L. (2014) NAD$^+$ and sirtuins in aging and disease. *Trends Cell Biol.* **24,** 464–471 CrossRef Medline
5. Garten, A., Schuster, S., Penke, M., Gorski, T., de Giorgis, T., and Kiess, W. (2015) Physiological and pathophysiological roles of NAMPT and NAD metabolism. *Nat. Rev. Endocrinol.* **11,** 535–546 CrossRef Medline
6. Verdin, E. (2015) NAD$^+$ in aging, metabolism, and neurodegeneration. *Science* **350,** 1208–1213 CrossRef Medline
7. Cantó, C., Menzies, K. J., and Auwerx, J. (2015) NAD$^+$ metabolism and the control of energy homeostasis: a balancing act between mitochondria and the nucleus. *Cell Metab.* **22,** 31–53 CrossRef Medline
8. Yang, Y., and Sauve, A. A. (2016) NAD$^+$ metabolism: bioenergetics, signaling and manipulation for therapy. *Biochim. Biophys. Acta* **1864,** 1787–1800 CrossRef Medline
9. Liu, H. W., Smith, C. B., Schmidt, M. S., Cambronne, X. A., Cohen, M. S., Migaud, M. E., Brenner, C., and Goodman, R. H. (2018) Pharmacological bypass of NAD$^+$ salvage pathway protects neurons from chemotherapy-induced degeneration. *Proc. Natl. Acad. Sci. U.S.A* **115,** 10654–10659 CrossRef Medline
10. Poyan Mehr, A., Tran, M. T., Ralto, K. M., Leaf, D. E., Washco, V., Messmer, J., Lerner, A., Kher, A., Kim, S. H., Khoury, C. C., Herzig, S. J., Trovato, M. E., Simon-Tillaux, N., Lynch, M. R., Thadhani, R. I., *et al.* (2018) *De novo* NAD$^+$ biosynthetic impairment in acute kidney injury in humans. *Nat. Med.* **24,** 1351–1359 CrossRef Medline
11. Schwarcz, R., Bruno, J. P., Muchowski, P. J., and Wu, H. Q. (2012) Kynurenines in the mammalian brain: when physiology meets pathology. *Nat. Rev. Neurosci.* **13,** 465–477 CrossRef Medline
12. Brown, K. D., Maqsood, S., Huang, J. Y., Pan, Y., Harkcom, W., Li, W., Sauve, A., Verdin, E., and Jaffrey, S. R. (2014) Activation of SIRT3 by the NAD$^+$ precursor nicotinamide riboside protects from noise-induced hearing loss. *Cell Metab.* **20,** 1059–1068 CrossRef Medline
13. Williams, P. A., Harder, J. M., Foxworth, N. E., Cochran, K. E., Philip, V. M., Porciatti, V., Smithies, O., and John, S. W. (2017) Vitamin B3 modulates mitochondrial vulnerability and prevents glaucoma in aged mice. *Science* **355,** 756–760 CrossRef Medline
14. Lin, J. B., Kubota, S., Ban, N., Yoshida, M., Santeford, A., Sene, A., Nakamura, R., Zapata, N., Kubota, M., Tsubota, K., Yoshino, J., Imai, S. I., and Apte, R. S. (2016) NAMPT-mediated NAD$^+$ biosynthesis is essential for vision in mice. *Cell Rep.* **17,** 69–85 CrossRef Medline
15. Belenky, P., Racette, F. G., Bogan, K. L., McClure, J. M., Smith, J. S., and Brenner, C. (2007) Nicotinamide riboside promotes Sir2 silencing and extends lifespan via Nrk and Urh1/Pnp1/Meu1 pathways to NAD$^+$. *Cell* **129,** 473–484 CrossRef Medline
16. Panozzo, C., Nawara, M., Suski, C., Kucharczyka, R., Skoneczny, M., Bécam, A. M., Rytka, J., and Herbert, C. J. (2002) Aerobic and anaerobic NAD$^+$ metabolism in *Saccharomyces cerevisiae*. *FEBS Lett.* **517,** 97–102 CrossRef Medline
17. Emanuelli, M., Carnevali, F., Lorenzi, M., Raffaelli, N., Amici, A., Ruggieri, S., and Magni, G. (1999) Identification and characterization of YLR328W, the *Saccharomyces cerevisiae* structural gene encoding NMN adenylyltransferase: expression and characterization of the recombinant enzyme. *FEBS Lett.* **455,** 13–17 CrossRef Medline
18. Bieganowski, P., Pace, H. C., and Brenner, C. (2003) Eukaryotic NAD$^+$ synthetase Qns1 contains an essential, obligate intramolecular thiol glutamine amidotransferase domain related to nitrilase. *J. Biol. Chem.* **278,** 33049–33055 CrossRef Medline
19. Bieganowski, P., and Brenner, C. (2004) Discoveries of nicotinamide riboside as a nutrient and conserved NRK genes establish a Preiss-Handler independent route to NAD$^+$ in fungi and humans. *Cell* **117,** 495–502 CrossRef Medline
20. Lu, S. P., Kato, M., and Lin, S. J. (2009) Assimilation of endogenous nicotinamide riboside is essential for calorie restriction-mediated life span extension in *Saccharomyces cerevisiae*. *J. Biol. Chem.* **284,** 17110–17119 CrossRef Medline
21. Croft, T., James Theoga Raj, C., Salemi, M., Phinney, B. S., and Lin, S. J. (2018) A functional link between NAD$^+$ homeostasis and N-terminal protein acetylation in *Saccharomyces cerevisiae*. *J. Biol. Chem.* **293,** 2927–2938 CrossRef Medline
22. Ohashi, K., Kawai, S., and Murata, K. (2013) Secretion of quinolinic acid, an intermediate in the kynurenine pathway, for utilization in NAD$^+$ biosynthesis in the yeast *Saccharomyces cerevisiae*. *Eukaryot. Cell* **12,** 648–653 CrossRef Medline
23. Amaral, M., Outeiro, T. F., Scrutton, N. S., and Giorgini, F. (2013) The causative role and therapeutic potential of the kynurenine pathway in neurodegenerative disease. *J. Mol. Med.* **91,** 705–713 CrossRef Medline
24. Chang, K. H., Cheng, M. L., Tang, H. Y., Huang, C. Y., Wu, Y. R., and Chen, C. M. (2018) Alternations of metabolic profile and kynurenine metabolism in the plasma of Parkinson's disease. *Mol. Neurobiol.* **55,** 6319–6328 CrossRef Medline
25. Ohashi, K., Chaleckis, R., Takaine, M., Wheelock, C. E., and Yoshida, S. (2017) Kynurenine aminotransferase activity of Aro8/Aro9 engage tryptophan degradation by producing kynurenic acid in *Saccharomyces cerevisiae*. *Sci. Rep.* **7,** 12180 CrossRef Medline
26. Lu, S. P., and Lin, S. J. (2011) Phosphate-responsive signaling pathway is a novel component of NAD$^+$ metabolism in *Saccharomyces cerevisiae*. *J. Biol. Chem.* **286,** 14271–14281 CrossRef Medline
27. Jungmann, J., Reins, H. A., Lee, J., Romeo, A., Hassett, R., Kosman, D., and Jentsch, S. (1993) MAC1, a nuclear regulatory protein related to Cu-dependent transcription factors is involved in Cu/Fe utilization and stress resistance in yeast. *EMBO J.* **12,** 5051–5056 CrossRef Medline
28. Graden, J. A., and Winge, D. R. (1997) Copper-mediated repression of the activation domain in the yeast Mac1p transcription factor. *Proc. Natl. Acad. Sci. U.S.A.* **94,** 5550–5555 CrossRef Medline
29. Gross, C., Kelleher, M., Iyer, V. R., Brown, P. O., and Winge, D. R. (2000) Identification of the copper regulon in *Saccharomyces cerevisiae* by DNA microarrays. *J. Biol. Chem.* **275,** 32310–32316 CrossRef Medline
30. Bedalov, A., Hirao, M., Posakony, J., Nelson, M., and Simon, J. A. (2003) NAD$^+$-dependent deacetylase Hst1p controls biosynthesis and cellular NAD$^+$ levels in *Saccharomyces cerevisiae*. *Mol. Cell. Biol.* **23,** 7044–7054 CrossRef Medline
31. Smith, J. S., Brachmann, C. B., Celic, I., Kenna, M. A., Muhammad, S., Starai, V. J., Avalos, J. L., Escalante-Semerena, J. C., Grubmeyer, C., Wolberger, C., and Boeke, J. D. (2000) A phylogenetically conserved NAD$^+$-dependent protein deacetylase activity in the Sir2 protein family. *Proc. Natl. Acad. Sci. U.S.A.* **97,** 6658–6663 CrossRef Medline




ASBMB

32. Llorente, B., and Dujon, B. (2000) Transcriptional regulation of the *Saccharomyces cerevisiae* DAL5 gene family and identification of the high affinity nicotinic acid permease TNA1 (YGR260w). *FEBS Lett.* **475,** 237–241 CrossRef Medline
33. Li, M., Petteys, B. J., McClure, J. M., Valsakumar, V., Bekiranov, S., Frank, E. L., and Smith, J. S. (2010) Thiamine biosynthesis in *Saccharomyces cerevisiae* is regulated by the NAD$^+$-dependent histone deacetylase Hst1. *Mol. Cell. Biol.* **30,** 3329–3341 CrossRef Medline
34. Sporty, J., Lin, S. J., Kato, M., Ognibene, T., Stewart, B., Turteltaub, K., and Bench, G. (2009) Quantitation of NAD$^+$ biosynthesis from the salvage pathway in *Saccharomyces cerevisiae*. *Yeast* **26,** 363–369 CrossRef Medline
35. To-e, A, Ueda, Y., Kakimoto, S. I., and Oshima, Y. (1973) Isolation and characterization of acid phosphatase mutants in *Saccharomyces cerevisiae*. *J. Bacteriol.* **113,** 727–738 Medline
36. Jensen, L. T., Posewitz, M. C., Srinivasan, C., and Winge, D. R. (1998) Mapping of the DNA binding domain of the copper-responsive transcription factor Mac1 from *Saccharomyces cerevisiae*. *J. Biol. Chem.* **273,** 23805–23811 CrossRef Medline
37. Serpe, M., Joshi, A., and Kosman, D. J. (1999) Structure-function analysis of the protein-binding domains of Mac1p, a copper-dependent transcriptional activator of copper uptake in *Saccharomyces cerevisiae*. *J. Biol. Chem.* **274,** 29211–29219 CrossRef Medline
38. Cankorur-Cetinkaya, A., Eraslan, S., and Kirdar, B. (2016) Transcriptomic response of yeast cells to ATX1 deletion under different copper levels. *BMC Genomics* **17,** 489 CrossRef Medline
39. De Freitas, J. M., Kim, J. H., Poynton, H., Su, T., Wintz, H., Fox, T., Holman, P., Loguinov, A., Keles, S., van der Laan, M., and Vulpe, C. (2004) Exploratory and confirmatory gene expression profiling of mac1Δ. *J. Biol. Chem.* **279,** 4450–4458 CrossRef Medline
40. Yamaguchi-Iwai, Y., Serpe, M., Haile, D., Yang, W., Kosman, D. J., Klausner, R. D., and Dancis, A. (1997) Homeostatic regulation of copper uptake in yeast via direct binding of MAC1 protein to upstream regulatory sequences of FRE1 and CTR1. *J. Biol. Chem.* **272,** 17711–17718 CrossRef Medline
41. Labbé, S., Zhu, Z., and Thiele, D. J. (1997) Copper-specific transcriptional repression of yeast genes encoding critical components in the copper transport pathway. *J. Biol. Chem.* **272,** 15951–15958 CrossRef Medline
42. Li, M., Valsakumar, V., Poorey, K., Bekiranov, S., and Smith, J. S. (2013) Genome-wide analysis of functional sirtuin chromatin targets in yeast. *Genome Biol.* **14,** R48 CrossRef Medline
43. Jackson, M. D., Schmidt, M. T., Oppenheimer, N. J., and Denu, J. M. (2003) Mechanism of nicotinamide inhibition and transglycosidation by Sir2 histone/protein deacetylases. *J. Biol. Chem.* **278,** 50985–50998 CrossRef Medline
44. Bitterman, K. J., Anderson, R. M., Cohen, H. Y., Latorre-Esteves, M., and Sinclair, D. A. (2002) Inhibition of silencing and accelerated aging by nicotinamide, a putative negative regulator of yeast sir2 and human SIRT1. *J. Biol. Chem.* **277,** 45099–45107 CrossRef Medline
45. Foster, A. C., Zinkand, W. C., and Schwarcz, R. (1985) Quinolinic acid phosphoribosyltransferase in rat brain. *J. Neurochem.* **44,** 446–454 CrossRef Medline
46. Kalikin, L., and Calvo, K. C. (1988) Inhibition of quinolinate phosphoribosyl transferase by pyridine analogs of quinolinic acid. *Biochem. Biophys. Res. Commun.* **152,** 559–564 CrossRef Medline
47. Gilmore, J. M., Sardiu, M. E., Venkatesh, S., Stutzman, B., Peak, A., Seidel, C. W., Workman, J. L., Florens, L., and Washburn, M. P. (2012) Characterization of a highly conserved histone related protein, Ydl156w, and its functional associations using quantitative proteomic analyses. *Mol. Cell. Proteomics* **11,** M111.011544 CrossRef Medline
48. Gavin, A. C., Bösche, M., Krause, R., Grandi, P., Marzioch, M., Bauer, A., Schultz, J., Rick, J. M., Michon, A. M., Cruciat, C. M., Remor, M., Höfert, C., Schelder, M., Brajenovic, M., Ruffner, H., *et al.* (2002) Functional organization of the yeast proteome by systematic analysis of protein complexes. *Nature* **415,** 141–147 CrossRef Medline
49. Zhu, Z., Labbé, S., Peña, M. M., and Thiele, D. J. (1998) Copper differentially regulates the activity and degradation of yeast Mac1 transcription factor. *J. Biol. Chem.* **273,** 1277–1280 CrossRef Medline
50. Iwai, K., and Taguchi, H. (1980) Crystallization and properties of quinolinate phosphoribosyltransferase from hog liver. *Methods Enzymol.* **66,** 96–101 CrossRef Medline
51. González Esquivel, D., Ramírez-Ortega, D., Pineda, B., Castro, N., Ríos, C., and Pérez de la Cruz, V. (2017) Kynurenine pathway metabolites and enzymes involved in redox reactions. *Neuropharmacology* **112,** 331–345 CrossRef Medline
52. Lu, S. P., and Lin, S. J. (2010) Regulation of yeast sirtuins by NAD$^+$ metabolism and calorie restriction. *Biochim. Biophys. Acta* **1804,** 1567–1575 CrossRef Medline
53. Braidy, N., and Grant, R. (2017) Kynurenine pathway metabolism and neuroinflammatory disease. *Neural Regen. Res.* **12,** 39–42 CrossRef Medline
54. Katsyuba, E., Mottis, A., Zietak, M., De Franco, F., van der Velpen, V., Gariani, K., Ryu, D., Cialabrini, L., Matilainen, O., Liscio, P., Giacchè, N., Stokar-Regenscheit, N., Legouis, D., de Seigneux, S., Ivanisevic, J., *et al.* (2018) *De novo* NAD$^+$ synthesis enhances mitochondrial function and improves health. *Nature* **563,** 354–359 CrossRef Medline
55. Breda, C., Sathyasaikumar, K. V., Sograte Idrissi, S., Notarangelo, F. M., Estranero, J. G., Moore, G. G., Green, E. W., Kyriacou, C. P., Schwarcz, R., and Giorgini, F. (2016) Tryptophan-2,3-dioxygenase (TDO) inhibition ameliorates neurodegeneration by modulation of kynurenine pathway metabolites. *Proc. Natl. Acad. Sci. U.S.A.* **113,** 5435–5440 CrossRef Medline
56. Mole, D. J., Webster, S. P., Uings, I., Zheng, X., Binnie, M., Wilson, K., Hutchinson, J. P., Mirguet, O., Walker, A., Beaufils, B., Ancellin, N., Trottet, L., Bénéton, V., Mowat, C. G., Wilkinson, M., *et al.* (2016) Kynurenine-3-monooxygenase inhibition prevents multiple organ failure in rodent models of acute pancreatitis. *Nat. Med.* **22,** 202–209 CrossRef Medline
57. Brachmann, C. B., Davies, A., Cost, G. J., Caputo, E., Li, J., Hieter, P., and Boeke, J. D. (1998) Designer deletion strains derived from Saccharomyces cerevisiae S288C: a useful set of strains and plasmids for PCR-mediated gene disruption and other applications. *Yeast* **14,** 115–132 CrossRef Medline
58. Burke, D., Dawson, D., and Sterns, T. (2000) *Methods in Yeast Genetics*, Cold Spring Harbor Laboratory Press, pp. 171–174, Cold Spring Harbor, NY
59. Güldener, U., Heck, S., Fielder, T., Beinhauer, J., and Hegemann, J. H. (1996) A new efficient gene disruption cassette for repeated use in budding yeast. *Nucleic Acids Res.* **24,** 2519–2524 CrossRef Medline
60. Goldstein, A. L., and McCusker, J. H. (1999) Three new dominant drug resistance cassettes for gene disruption in *Saccharomyces cerevisiae*. *Yeast* **15,** 1541–1553 CrossRef Medline
61. Longtine, M. S., McKenzie, A., 3rd, Demarini, D. J., Shah, N. G., Wach, A., Brachat, A., Philippsen, P., and Pringle, J. R. (1998) Additional modules for versatile and economical PCR-based gene deletion and modification in *Saccharomyces cerevisiae*. *Yeast* **14,** 953–961 CrossRef Medline
62. Easlon, E., Tsang, F., Skinner, C., Wang, C., and Lin, S. J. (2008) The malate-aspartate NADH shuttle components are novel metabolic longevity regulators required for calorie restriction-mediated life span extension in yeast. *Genes Dev.* **22,** 931–944 CrossRef Medline
63. Winzeler, E. A., Shoemaker, D. D., Astromoff, A., Liang, H., Anderson, K., Andre, B., Bangham, R., Benito, R., Boeke, J. D., Bussey, H., Chu, A. M., Connelly, C., Davis, K., Dietrich, F., Dow, S. W., *et al.* (1999) Functional characterization of the *S. cerevisiae* genome by gene deletion and parallel analysis. *Science* **285,** 901–906 CrossRef Medline
64. Kato, M., and Lin, S. J. (2014) YCL047C/POF1 is a novel nicotinamide mononucleotide adenylyltransferase (NMNAT) in *Saccharomyces cerevisiae*. *J. Biol. Chem.* **289,** 15577–15587 CrossRef Medline